

High Redshift Galaxies in the Hubble Deep Field: II. Colours and Number Counts

Lucia Pozzetti^{1,2,3}, Piero Madau³, Gianni Zamorani^{2,4}, Henry C. Ferguson³, & Gustavo A. Bruzual⁵

¹*Dipartimento di Astronomia, Università di Bologna, via Zamboni 33, I-40126 Bologna, Italy (lucia@astbo3.bo.astro.it)*

²*Osservatorio Astronomico di Bologna, via Zamboni 33, I-40126 Bologna, Italy*

³*Space Telescope Science Institute, 3700 San Martin Drive, Baltimore, MD 21218, USA*

⁴*Istituto di Radioastronomia del CNR, via Gobetti 101, I-40129 Bologna, Italy*

⁵*Centro de Investigaciones de Astronomía, A.P. 264, Mérida 5101-A, Venezuela*

Accepted 0000 xxxxxxxx 00. Received 0000 xxxxxxxx 00; in original form 0000 xxxxxxxx 00

ABSTRACT

We discuss the deep galaxy counts from the *Hubble Deep Field* (HDF) imaging survey. At faint magnitudes, the slope of the differential number-magnitude relation is flatter than 0.2 in all four HDF bandpasses. In the ultraviolet, a fluctuation analysis shows that the flattening observed below $U_{300} \approx 26$ mag is not due to incompleteness and is more pronounced than in the other bands, consistent with the idea that a redshift limit has been reached in the galaxy distribution. A reddening trend of ≈ 0.5 magnitude is observed at faint fluxes in the colour-magnitude diagram, $(U_{300} - V_{606})_{eff}$ versus V_{606} . We interpret these results as the effect of intergalactic attenuation on distant galaxies. At flux levels of $AB \approx 27$ mag and in agreement with the fluctuation analysis and the colour-magnitude relation, about 7% of the sources in U_{300} , 30% in B_{450} and 35% in V_{606} are Lyman-break “dropouts”, i.e. candidate star-forming galaxies at $z > 2$. By integrating the number counts to the limits of the HDF survey we find that the mean surface brightness of the extragalactic sky is dominated by galaxies that are relatively bright and are known to have $\langle z \rangle \sim 0.6$. To $AB \approx 29$ mag, the integrated light from resolved galaxies in the I -band is $2.1_{-0.3}^{+0.4} \times 10^{-20}$ erg cm⁻² s⁻¹ Hz⁻¹ sr⁻¹, and its spectrum is well described by a broken power-law ($I_\nu \propto \lambda^2$ from 2000 to 8000 Å and $I_\nu \propto \lambda$ from 8000 to 22000 Å). We discuss the predictions for the counts, colours, and luminosity densities from standard low- q_0 pure-luminosity-evolution models without dust obscuration, and find that they are unable to reproduce all the observed properties of faint field galaxies.

Key words: cosmology: miscellaneous – galaxies: evolution – intergalactic medium – quasars: absorption lines – ultraviolet: galaxies

1 INTRODUCTION

As the best view to date of the optical sky at faint flux levels, the *Hubble Deep Field* (HDF) imaging survey has rapidly become a key testing ground for models of galaxy evolution. With its depth – reaching 5- σ limiting AB magnitudes of roughly 27.7, 28.6, 29.0, and 28.4 in the F300W, F450W, F606W, and F814W bandpasses (Williams et al. 1996) – and four-filter strategy in order to detect Lyman-break galaxies at various redshifts, the HDF offers the opportunity to study the galaxy population in unprecedented detail. In particular, the great cosmological importance of measuring the number-magnitude relation (and its first moment, the integrated extragalactic background light) and the colour distribution at the faintest detection limits reached by the HDF stems from the prospect of using them as a probe of

the cosmic history of star formation in galaxies (Metcalf et al. 1996; Ferguson & Babul 1997).

At faint magnitudes, the interpretation and detailed modeling of the observations require the self-consistent inclusion of the effect of intergalactic attenuation on galaxy counts and colours. Absorption by intervening material has been known for quite some time to distort our view of objects at cosmological distances. It has been realized only recently, however, that the increasing opacity of the intergalactic medium (IGM) at high redshifts can be efficiently used to identify galaxies at $z \gtrsim 2$. As shown by Madau (1995) (see also Yoshii & Peterson 1994), the accumulated Lyman-continuum absorption from the Ly α forest clouds and Lyman-limit systems along the path is so severe that galaxies beyond $z \approx 3$ become effectively undetectable in the ultraviolet. Similarly, at $z \approx 3.5$, the

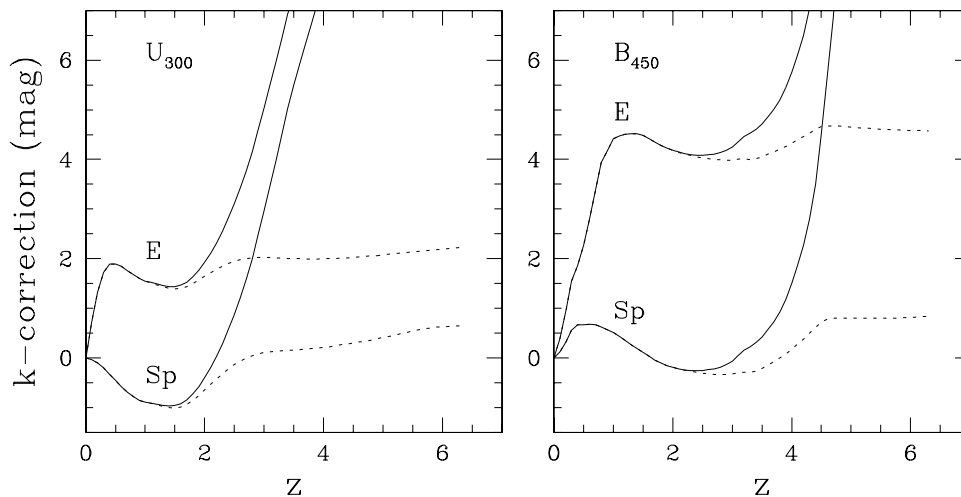


Figure 1. Average k -corrections in the U_{300} and B_{450} bands for elliptical and late-type spiral galaxies as a function of redshift. *Dotted lines:* unattenuated synthetic spectra. *Solid lines:* spectra modified by intergalactic absorption.

blanketing by discrete absorption lines in the Lyman series is so effective that galaxies appear about 1 mag fainter in the blue. Ground-based observations have used colour techniques which are sensitive to the presence of a Lyman-continuum break superposed to an otherwise flat UV spectrum to identify or set limits on the number of high redshift galaxies (Guhathakurta, Tyson, & Majewski 1990; Steidel & Hamilton 1992; Steidel et al. 1996a). Specific colour selection criteria which exploit the ubiquitous effect of intergalactic absorption and provide a robust separation between high-redshift and low-redshift galaxies have been developed for the HDF bandpasses by Madau et al. (1996).

The magnitude and cosmological importance of intergalactic absorption on galaxy number counts can be effectively illustrated by including its effect in the standard k -correction term needed to translate the galaxy magnitude at Earth into its rest-frame value. Assuming no intrinsic luminosity evolution, the mean k -correction is

$$k(z) = -2.5 \log \left[(1+z) \frac{L(\nu_{\text{em}})}{L(\nu_{\text{obs}})} \langle e^{-\tau} \rangle \right], \quad (1)$$

where $L(\nu_{\text{em}})$ is the specific power emitted by a source at redshift z , $\nu_{\text{obs}} = \nu_{\text{em}}/(1+z)$, and $\langle e^{-\tau} \rangle$ is the cosmic transmission averaged over all lines of sight. Figure 1 shows the average k -correction in the U_{300} and B_{450} bands as a function of redshift for synthetic spectra of galaxies (based on Bruzual & Charlot’s 1993 libraries) which well reproduce the colours of present-day ellipticals and late-type spirals. The effect at high redshifts is huge. Due to intergalactic attenuation alone, the average k -correction in the F300W bandpass increases by more than 4 magnitudes between $z \approx 2$ and $z \approx 3.5$, giving origin to a “UV dropout”. In the F450W band, the increase is only noticeable above $z \approx 3$, but becomes very large above $z \approx 4$ (producing a “blue dropout”). Qualitatively, the inclusion of intergalactic attenuation in any galaxy evolution model will cause a flattening, more pronounced in the bluest bands, of the slope of the number-magnitude relation and a reddening of the ultraviolet-optical colours.

In this paper we will focus on the $N(m)$ relation in the U_{300} , B_{450} , V_{606} , and I_{814} HDF bandpasses. A fluctuation analysis on the U_{300} image allows us to estimate the slope of the ultraviolet number counts below the nominal detection limit. These are found to flatten significantly below 26 mag, while a reddening trend of ≈ 0.5 mag is observed in the colour-magnitude diagram, $(U_{300} - V_{606})_{\text{eff}}$ versus V_{606} . Both these results are consistent with the idea that, at flux limits fainter than 27 mag, high- z galaxies make a significant contribution to the counts in the redder bands, in agreement with an extension to faint magnitudes of the “dropout” colour technique. We compute the extragalactic background light (EBL) from discrete sources, and find that it can be well described by a broken power-law, $I_\nu \propto \lambda^2$ between 2000 and 8000 Å, and $I_\nu \propto \lambda$ between 8000 and 22000 Å. Relatively bright galaxies at the limit of existing spectroscopic surveys are responsible for about 60% of the sky brightness. Finally, we examine a representative ($H_0 = 50$ km s $^{-1}$ Mpc $^{-1}$, $q_0 = 0.05$) pure-luminosity-evolution (hereafter PLE) model without dust obscuration, and show that this is unable to reproduce all the observed properties of faint galaxies. In particular, it overpredicts the fraction of $z \gtrsim 3$ objects and fails to account for the steep observed trend of the comoving luminosity density in the interval $0 < z < 1$ at all wavelengths.

Throughout this paper, all magnitudes will be given in the AB system (Oke 1974).

2 THE HUBBLE DEEP FIELD

The HDF observations allow us to statistically analyze the high- z galaxy population at magnitudes much fainter than current spectroscopic limits. In this section, we shall use the number counts, the Lyman-break dropout technique, and the colour-magnitude diagram to assess the effects of an absorption-induced loss of sources in the ultraviolet and blue bands.

The galaxy sample we use, extracted from Version 2 of the HDF catalog, consists of 2819 objects detected in

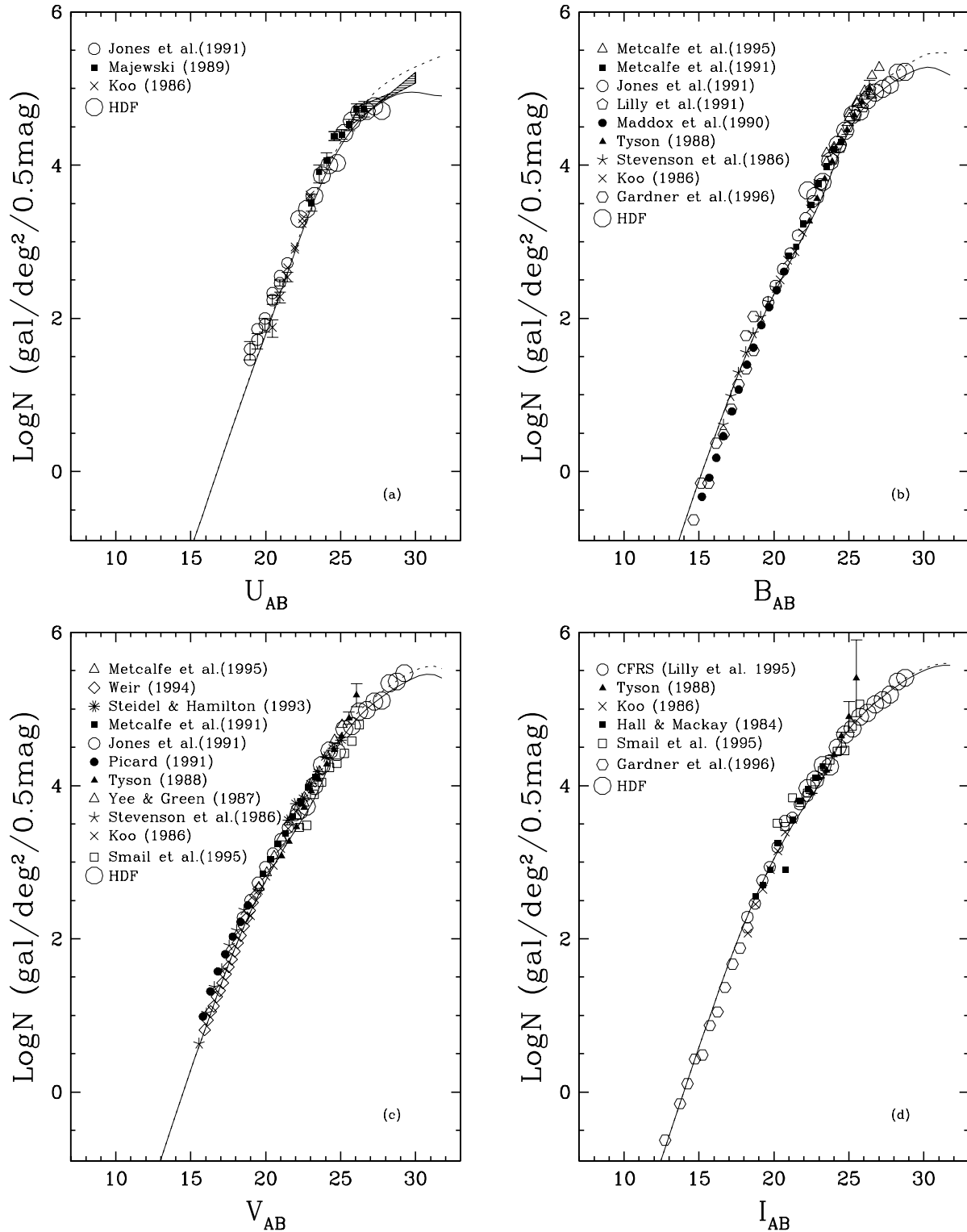


Figure 2. Differential U , B , V , and I galaxy counts as a function of AB magnitudes. The sources of the data points are indicated in each panel. Note the decrease of the logarithmic slope $d\log N/dm$ at faint magnitudes. The flattening is more pronounced at the shortest wavelengths. The lines show the predicted counts for a PLE model ($H_0 = 50 \text{ Km s}^{-1} \text{ Mpc}^{-1}$, $q_0 = 0.05$), with (solid line) and without (dotted line) the inclusion of intergalactic absorption. The shaded region in panel (a) shows the results of our “fluctuation analysis” (see text).

the three WF chips from the F606W+F814W summed images. The detection threshold was set to $4\sigma_{sky}$, and the minimum area to 25 drizzled pixels (Williams et al. 1996). Magnitudes or upper limits in each band were computed from an area corresponding to the limiting isophote of the summed F606W+F814W image. Details of the data reduction, source detection algorithm, and photometry are given in Williams et al. (1996), together with the angular separation and colour criteria adopted for the merging of subcomponents. It is important to keep in mind that the results discussed below refer to a red-selected sample: in principle, objects with very blue colours, due for example to strong emission lines in the F300W or F450W bandpass, may have escaped detection if their red $V_{606} + I_{814}$ magnitudes do not satisfy the selection criteria.

Figure 2 shows the HDF galaxy counts as a function of AB isophotal magnitudes in the F300W, F450W, F606W, and F814W bandpasses, as derived by Williams et al. (1996) for all galaxies with signal-to-noise ratio $S/N > 3$ within the band. At this limit the counts are likely to be more than 80% complete. A compilation of existing ground-based data is also shown. All the surveys have been corrected to AB magnitudes, while the second order colour corrections for the differences in the filter effective wavelengths have not been applied to the ground-based data. For the typical colours of galaxies in the HDF, these corrections are less than 0.1 mag. The HDF counts agree reasonably well with previous surveys, to within 20% in the magnitude range $22 < AB < 26$. At faint fluxes, however, the Williams et al. counts in the four individual passbands are lower by about 30% than those obtained for the HDF by Metcalfe et al. (1996). A detailed comparison of the Williams et al. and Metcalfe et al. catalogs reveals several significant differences. First, there are systematic discrepancies in the total magnitudes of the galaxies. At $V_{606} = 25 \pm 0.5$, the median shift (Metcalfe–Williams) is -0.01 mag. This grows to about -0.20 mag at fainter fluxes ($V_{606} = 28 \div 29$), and is probably due to different algorithms used for “growing” the photometry beyond the outer isophotes of the galaxies. A further difference between the two catalogs is the amount of splitting near bright objects, as these are split into slightly more pieces in the Metcalfe et al. catalog than in Williams et al. Finally, the Metcalfe et al. sample contains sources with lower S/N than the Williams et al. sample. As the error on the magnitudes near the detection threshold is ~ 0.5 mag, the slightly fainter detection limit will tend to steepen the counts, even a magnitude or so above the nominal depth of the catalog. These three effects probably account for most of the discrepancies, and we believe are indicative of the possible systematic errors that are inherent in *HST* faint-galaxy photometry.

It is important to note that, in all four HDF bands, the slope of the differential number-magnitude relation is flatter than 0.2 below $AB = 26$ mag, as previously found by other authors (Williams et al. 1996; Metcalfe et al. 1996), and that this flattening is more pronounced at the shorter wavelengths. We will show in Section 2.2, through a fluctuation analysis, that the turnover observed in the U_{300} band is not due to incompleteness, but it is consistent with the idea that, at faint magnitudes in the red bands, a significant fraction of galaxies are actually at high redshifts, and are therefore “reddened” by absorbing material along the

line of sight.

2.1 Biases

We should caution the reader that there are a number of subtle effects that can affect the photometry at very faint magnitudes, especially in the U_{300} band. First, the charge transfer efficiency (CTE) of the WFPC-2 CCD is not perfect, and can lead to magnitudes that are systematically too faint for sources observed at low count rates with low background. For the typical background levels of 1 DN for the F300W exposures, the average CTE correction is ~ 0.03 magnitudes for galaxies with $U_{300} \approx 25$. This correction will depend on the location of the source on the chip, varying from zero at low row numbers to 0.5 mag near the top of the chip. The CTE effect on sources several magnitudes fainter is not well calibrated, but is unlikely to be more than 0.1 mag. A second subtlety is that, at background levels of ~ 1 DN per exposure, the determination of the local background for a galaxy is affected by the discrete steps of the CCD analog-to-digital converter. While the algorithm used by FOCAS (a clipped mean) should be a good estimator of the background, we have not tested this ourselves on simulated data. Finally, for galaxy fluxes within several percent of the background, it is possible that systematic biases creep in due to the different treatment of the pixel intensities in the source aperture and background region. In particular, the mean intensity in the local-background region is determined after clipping out pixels more than 10 sigma away from an initial estimate of the mean, while the flux in the source aperture is an unclipped sum of the counts. This could bias the fluxes of sources that are very faint in F300W towards slightly higher values, resulting in measured colours somewhat bluer than the true colours. Finally, at magnitude levels fainter than $V_{606} = 28$, it is likely that even objects which are brighter than the nominal depth of the catalog may be missed due to low surface brightness. These galaxies could be preferentially either blue or red. For example, high redshift galaxies that are not forming stars rapidly will be red and have quite low surface brightness. The $(1+z)^4$ dimming effect is equal to 1.2 magnitudes between $z = 2$ and $z = 3$. On the other hand, locally, LSB galaxies tend to be quite blue. A relatively local population of LSB galaxies could in principle exist and the fainter examples could disappear below the HDF sky background.

With these caveats in mind, we will limit our analysis to galaxies with $V_{606} < 29$ mag, with the expectation that systematic biases will be significantly less than ~ 0.5 mag in the photometry, and less than $\sim 50\%$ in the galaxy counts.

2.2 Fluctuation Analysis

As the F300W bandpass is sensitive to intergalactic attenuation at $z \gtrsim 2$, deep counts in this band are essential for estimating, through the comparison with counts at longer wavelengths, the number of high- z galaxies in a red-selected sample, and for deriving constraints on models of galaxy evolution.

The published UV $N(m)$ (Williams et al. 1996) already suggests a sharp flattening from a logarithmic slope of $d \log N/dm \approx 0.40$ at $U_{300} \leq 26$ mag to a slope consistent with zero for $26 < U_{300} < 28$. In principle, however, this

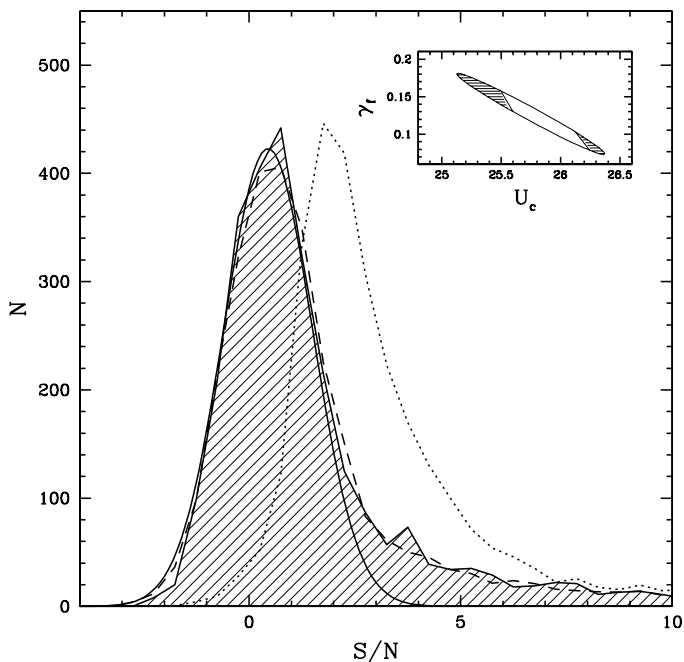


Figure 3. S/N distribution in the U_{300} band. The data (shaded region) are compared to a simulated distribution with $U_c = 25.75$ mag, and $\gamma_f = 0.135$ (dashed line) or 0.350 (dotted line). The gaussian curve represents the expected distribution for undetected objects (see text). The upper right panel shows the 95% confidence region for the parameters U_c and γ_f from a KS test (see text).

sharp flattening could also be due to significant incompleteness in the faintest U_{300} bins. Note that, since the limiting ultraviolet flux is about one magnitude brighter than in the other bands, the fraction of galaxies in the catalog that are undetected (i.e. $S/N < 3$) in the F300W bandpass is very large ($\sim 80\%$), and it is difficult to draw statistically reliable conclusions from the raw data.

In the attempt to push the U_{300} counts to even fainter magnitudes, we have therefore applied a “fluctuation analysis” to the Version 2 catalog data. The simplest possible model for the differential counts has been assumed, i.e. a double power-law characterized by four parameters: the overall normalization (A), two slopes (γ_b and γ_f at bright and faint magnitudes, respectively), and the magnitude (U_c) of the turnover. While two of them (A and γ_b) have been kept fixed by requiring a good fit to the bright HDF $N(m)$, we have determined a best estimate for the other two parameters (γ_f and U_c) in the following way:

- values for the ultraviolet magnitudes of the sources have been randomly extracted from the input $N(m)$;
- the corresponding “measured” counts for each galaxy have been derived assuming Poisson statistics;
- an isophotal area has been assigned to each object, on the basis of the correlation between area and magnitude observed in the catalog, and the corresponding number of background counts has been derived;
- finally, a signal-to-noise ratio [$S/N = L_i/\sigma(L_i)$] has been computed according to the formula (Note that in equation 6 in Williams et al. 1996 there was a typo in the second

and third terms):

$$[\Gamma\sigma(L_i)]^2 = \Gamma N_{obj} + 1.9^2 \Gamma^2 \sigma_{sky}^2 A_{obj} + 1.9^2 \Gamma^2 \sigma_{sky}^2 A_{obj}^2 / A_{sky}, \quad (2)$$

where L_i is the sky-subtracted number of counts within the detection isophote, Γ is the inverse gain, N_{obj} is the total number of counts in the object aperture, A_{obj} and A_{sky} are the areas within the source and sky apertures, and σ_{sky} is the measured standard deviation of the background within the sky aperture (cf. Williams et al. 1996).

By repeating these steps a large number of times (10,000), we have constructed a simulated distribution of signal-to-noise ratios for each input $N(m)$, and these distributions have then been compared to the observed one for all the 2819 objects of the merged catalog. Figure 3 shows such a comparison for $U_c = 25.75$. As expected, the observed distribution can be described as a gaussian at low S/N values, which represents the expected distribution for undetected objects, plus a tail at high S/N values. Since these are computed not in random positions, but at the positions where galaxies are detected in the red bands, the gaussian-like distribution is not centered around zero, but is displaced toward a higher value ($S/N \sim 0.5$). The two curves plotted in Figure 3 show the results of two simulations, corresponding to the slopes of $\gamma_f = 0.380$ and $\gamma_f = 0.135$. The case $\gamma_f \sim \gamma_b \sim 0.4$ is clearly ruled out to a high degree of significance. From a KS statistical test the formal 95% confidence region for (U_c, γ_f) can actually be derived. The two parameters are obviously highly correlated, with steeper slopes allowed for brighter values of U_c and vice-versa (see inset in the upper right corner of Figure 3). Note, however, that the region in the upper left part of the 95% confidence ellipse produces number counts which are lower than the observed ones for $25.75 \leq U_{300} \leq 27.25$, while its lower right part produces counts which are higher than the observed ones in the same magnitude range. By requiring the models to be consistent with the data to better than 5% in the four bins between $25.75 \leq U_{300} \leq 27.25$, the two hatched regions of the parameter space can be further excluded, and the allowed ranges become $25.6 < U_c < 26.2$ and $0.08 < \gamma_f < 0.16$. The best-fit values are $U_c = 25.75$, and $\gamma_f = 0.135$. The latter is steeper than the value of 0.05 quoted in Williams et al. (1996), but still flatter than the corresponding values for the B_{450} , V_{606} , I_{814} bands, as expected in the case of a significant absorption-induced loss of faint, distant sources.

All the allowed models predict a number of galaxies between 20 to 30% higher than observed in the faintest bin quoted by Williams et al. (1996), $27.5 < U_{300} < 28.0$. The Version 2 catalog contains 112 galaxies in this magnitude bin, with only 79 satisfying the $S/N \geq 3$ constraint used by Williams et al. in deriving their counts. This suggests some incompleteness in the Williams et al. counts at this magnitude level. Since the catalog has been derived using isophotal magnitudes and the isophotal areas are defined in the red bandpasses, for galaxies with a given ultraviolet flux (i.e., with a given signal) there is an inverse correlation between S/N and isophotal area: smaller signal-to-noise ratios correspond to larger areas and therefore, in first approximation, to galaxies that are brighter in the red bands. For this reason, the sources eliminated because of the S/N constraint are not a random sub-sample of the galaxies in this

magnitude range, but correspond to those with the reddest $U_{300} - V_{606}$ and/or $U_{300} - I_{814}$ colours. This has to be taken into account if one analyzes the colour distribution of the galaxies in the faintest U_{300} magnitude bin of the catalog.

As mentioned in Section 2, galaxies with very blue colours, not selected in the catalog because fainter than the limits in $V_{606} + I_{814}$, could in principle contribute somewhat to the U_{300} counts. Because our analysis uses as input the red selected catalog, this contribution would not be accounted for in our extrapolated estimate of the U_{300} counts. Given the approximate limit in the V_{606} band ($V_{lim} \sim 29.0$), these “potential” blue objects could appear at $U_{300} \sim 29$ if they had $U_{300} - V_{606} \leq 0$ and at $U_{300} \sim 29.5$ if they had $U_{300} - V_{606} \leq 0.5$. In the “bright” part of the catalog (i.e. $V_{606} < 26$), where no such object is expected to have been lost, there is only 1% of the galaxies with $U_{300} - V_{606} \leq 0$ and only 12% of the galaxies with $U_{300} - V_{606} \leq 0.5$. On this basis we argue that our conclusion on the reality of the flattening in the U_{300} counts is robust and our estimate of the parameters of the slope down to $U_{300} \sim 29.5$ can be considered to be reliable.

2.3 Lyman-Break Dropouts and the High- z Luminosity Functions

Photometric criteria for robustly selecting Lyman-break galaxies in the HDF have been developed by Madau et al. (1996). They have been tuned up to provide what appear to be largely uncontaminated samples of star-forming galaxies at high redshifts, and have been refined (Madau 1997) after the many redshift measurements with the Keck telescope (Steidel et al. 1996b; Cohen et al. 1996; Lowenthal et al. 1997). The HDF ultraviolet passband – which is bluer than the standard ground-based U filter – permits the identification of star-forming galaxies in the interval $2 \lesssim z \lesssim 3.5$. Galaxies in this redshift range predominantly occupy the top left portion of the $U_{300} - B_{450}$ vs. $B_{450} - I_{814}$ colour-colour diagram because of the attenuation by the intergalactic medium and intrinsic absorption. Galaxies at lower redshift can have similar $U_{300} - B_{450}$ colours, but are typically either old or dusty, and are therefore red in $B_{450} - I_{814}$ as well. In analogous way, it is possible to single out star-forming galaxies at $3.5 \lesssim z \lesssim 4.5$ by looking at the $B_{450} - V_{606}$ vs. $V_{606} - I_{814}$ colour-colour diagram.

We have estimated the number of U_{300} and B_{450} dropouts as a function of V_{606} magnitudes by applying, with some modifications, the procedure described in Madau et al. (1996). The main differences with respect to Madau’s procedure are: i) We considered as detected only objects with $S/N \geq 2.5$, rather than $S/N \geq 1$ as in Madau’s analysis. For the objects with a lower S/N we computed a lower limit to the magnitude corresponding to $S/N = 2.5$. As seen in Figure 3, it is only for $S/N \geq 2.5$ that the observed distribution starts to depart significantly from the expected distribution of the noise, represented in the figure by the gaussian curve. Therefore, the objects with lower S/N can not be considered detections. ii) Since with this choice we have a higher number of lower limits in the colours, the number of dropouts in each V_{606} bin has been estimated using the Kaplan-Meier estimator in the package ASURV (La Valley, Isobe & Feigelson 1992), which implements the methods for a maximum-likelihood reconstruction of the true distri-

Table 1. Number of Lyman-break dropouts

| V_{606} bin | Udrops | Bdrops |
|---------------|------------------|----------------|
| 23.75 | 5.0 ± 1.9 | 0.0 |
| 24.25 | 6.0 ± 2.4 | 0.0 |
| 24.75 | 11.0 ± 2.7 | 0.0 |
| 25.25 | 16.9 ± 3.3 | 0.0 |
| 25.75 | 29.9 ± 4.2 | 1.0 ± 1.0 |
| 26.25 | 35.4 ± 5.3 | 3.0 ± 1.7 |
| 26.75 | 47.1 ± 7.1 | 2.5 ± 1.6 |
| 27.25 | 68.5 ± 9.2 | 5.0 ± 2.2 |
| 27.75 | – | 12.8 ± 6.8 |
| 23.5 ÷ 28.0 | 219.8 ± 14.6 | 24.3 ± 7.6 |

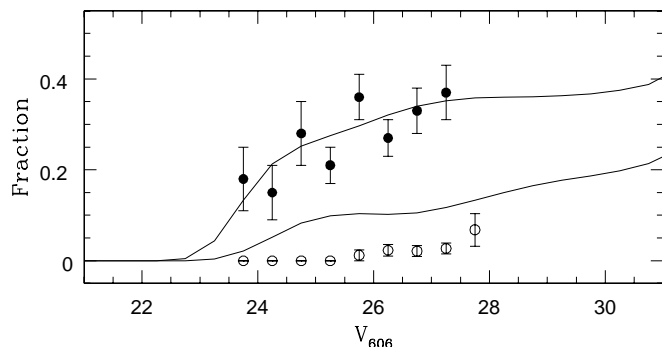


Figure 4. Fraction of high- z galaxies as a function of V_{606} magnitudes as obtained from a dropouts analysis, using the ASURV package. *Filled circles:* U_{300} -dropouts. *Empty circles:* B_{450} -dropouts. *Solid lines:* PLE model predictions.

bution function when limits are present (Feigelson & Nelson 1985). Table 1 shows the numbers of U_{300} dropouts for $V_{606} \leq 27.5$ and of B_{450} dropouts for $V_{606} \leq 28$ as a function of V_{606} magnitudes. At fainter V_{606} magnitudes the number of limits in U_{300} becomes greater than 60% of the total number of data points. For these high percentages of limits the performances of survival analysis statistics deteriorate and the results are not reliable anymore (Feigelson 1992). The corresponding fractions of dropouts are shown in Figure 4 as a function of V_{606} magnitudes in 0.5 magnitude bins. The fraction of $U + B$ dropouts varies from $\sim 5\%$ to 40% in the range $23.5 < V_{606} < 27.5$. The cumulative fraction of F300W-dropouts to $V_{606} < 27.5$ is $28 \pm 2\%$, while it is $2.5 \pm 0.6\%$ to $V_{606} < 28$ for the F450W-dropouts.

With a similar procedure we have computed the fraction of Lyman-break dropouts as a function of U_{300} and B_{450} magnitudes, finding that this decreases significantly in the U_{300} band. For example, at $AB \approx 27$, it is $\sim 7\%$ in U_{300} , while it is $\sim 30\%$ in B_{450} and $\sim 35\%$ in V_{606} .

The Kaplan-Meier estimator used in this analysis can be properly applied only in presence of a random censorship, i.e. in cases in which the distribution of the observational sensitivities for the non-detected objects is the same as that for the detections (Schmitt 1985, Magri et al. 1988). In our case this condition is satisfied, because for each magnitude bin in V_{606} the distribution of the thresholds in U_{300} is essentially a function of A_{obj} (see Eq. 2), which is not related to the variable to be measured (i.e. the U_{300} magnitude).

However, the non-parametric Kaplan-Meier reconstruction of the true distribution implicitly assumes also that the limits and the detections are drawn from the same parent distribution. Since we can not be sure that this assumption is true, we have analyzed the same data also with a maximum likelihood parametric method. Consistently with the analysis described in more detail in Section 2.4, we have assumed the following functional form for the distribution of the $U_{300} - B_{450}$ colours: a fraction f of the population of galaxies is highly absorbed in U_{300} and is described formally by a δ -function at a high value of $U_{300} - B_{450}$; a fraction $(1 - f)$ of the population is described by a gaussian distribution in $U_{300} - B_{450}$. The likelihood for this functional form can be easily derived (see Avni & Tananbaum 1986). Maximizing the likelihood function one can then obtain the best estimates for the three parameters (f plus the two describing the gaussian) and from these derive the best estimate for the number of dropouts, i.e. those satisfying the condition of having a $U_{300} - B_{450}$ color greater than the adopted threshold. The numbers derived with this procedure are all consistent, within one sigma, with those given in Table 1 in each magnitude bin. Since the assumptions in the two methods are significantly different, this suggests that our estimate of the number of dropouts is statistically robust.

As a test of the adopted colour selection window, we have compared our estimates of the fraction of bright UV dropouts in the HDF with the results from the B -selected spectroscopic sample described by Cowie et al. (1997). The latter covers, in the magnitude range $24 < B < 24.5$, about 13 arcmin^2 , and contains 42 galaxies, of which 4 have $z \gtrsim 2$, and 2 are still unidentified (and most likely lies at $z > 1.6$, Cowie et al. 1997). The fraction of spectroscopically identified galaxies at $z \gtrsim 2$ in the ground-based sample is therefore between 10 and 14%. This is in good agreement with our estimated fraction, $\sim 11\%$, of ultraviolet dropouts in the same magnitude range.

Using the numbers of dropouts as a function of magnitude, we have computed the luminosity functions (LF) of high- z galaxies in two different redshift ranges. The observed V_{606} and I_{814} magnitudes have been converted to intrinsic M_{1600} AB magnitudes, and the number densities of U_{300} and B_{450} dropouts have been obtained assuming that they sample the redshift intervals $2.0 < z < 3.5$ and $3.5 < z < 4.5$, respectively. The results are shown in Figure 5 ($H_0 = 50 \text{ km s}^{-1} \text{ Mpc}^{-1}$, $q_0 = 0.05$). The shape of the LF for the redshift interval $2.0 < z < 3.5$ is reasonably well defined and can be described by a Schechter function with parameters $\alpha = -1.3$, $M_{1600}^* = -21.7$ and $\Phi^* = 0.8 \times 10^{-3} \text{ Mpc}^{-3}$. For the higher redshift interval the fitting line shown in the figure has the same α and M_{1600}^* parameters, but a lower normalization ($\Phi^* = 0.2 \times 10^{-3} \text{ Mpc}^{-3}$). As a comparison, the thick curve in Figure 5 shows the local M_{1600} LF, derived from the Treyer et al. (1997) data. The high- z luminosity functions clearly extend to much brighter magnitudes, while no indication of a steep faint end slope is clearly seen in the HDF data. Even the HDF data, however, are not deep enough to exclude the possibility of a steepening at faint fluxes. The comoving luminosity density resulting from the integration to $M_{1600} = -18$ of the two HDF LF are $\rho_L = 2.0(\pm 0.5) \times 10^{19} \text{ W Hz}^{-1} \text{ Mpc}^{-3}$ for $2.0 < z < 3.5$, and $\rho_L = 5.2(\pm 2.6) \times 10^{18} \text{ W Hz}^{-1} \text{ Mpc}^{-3}$ for $3.5 < z < 4.5$,

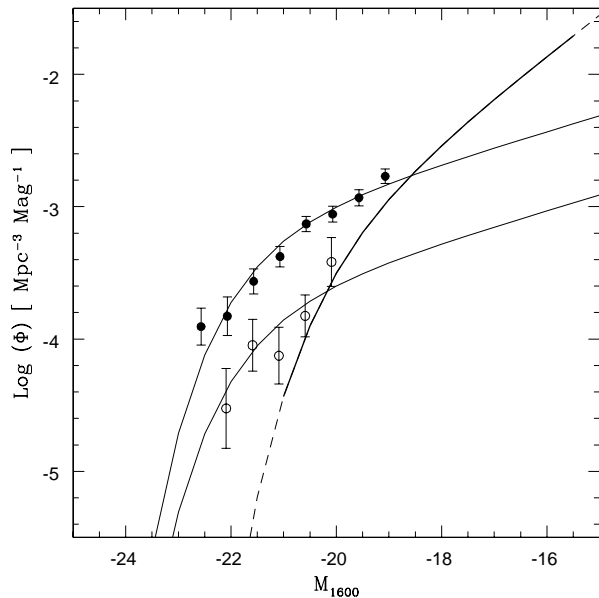


Figure 5. Luminosity function at 1600 \AA ($H_0 = 50 \text{ km s}^{-1} \text{ Mpc}^{-1}$, $q_0 = 0.05$). *Filled circles*: U_{300} -dropouts. *Empty circles*: B_{450} -dropouts. The solid lines represent Schechter fits to the data. The local luminosity function at 2000 \AA from Treyer et al. (1997) is also shown (*thick curve*).

in good agreement with the estimates of Madau (1997). The errors on ρ_L have been obtained by combining the statistical errors on the number of dropouts (see Table 1) with an estimated uncertainty of the volumes effectively sampled by the adopted colour selection techniques.

These luminosity functions (and the corresponding luminosity densities) should probably be considered as lower limits to the true ones. In fact, on the basis of an analysis of the spectra and colours of a representative, spectroscopically confirmed sample of high redshift star-forming galaxies, Pettini et al. (1997) have shown that the likely dust correction to the integrated ultraviolet luminosity for these galaxies is about a factor of 3. (Note that the Treyer et al. LF has not been corrected for extinction). Moreover, the dropout technique used in selecting our high redshift candidates works efficiently for galaxies for which the attenuation due to intergalactic matter is equal to or higher than the assumed average attenuation. Galaxies with a lower than average attenuation may well have ($U_{300} - B_{450}$) and ($B_{450} - V_{606}$) colours bluer than those used in selecting the high- z sample. Madau et al. (1996) have estimated that only about 20% of galaxies at $z > 2.7$ can be missed because of this effect. However, only extensive spectroscopic observations of galaxies lying below the colour threshold can provide a quantitative estimate of the size of this incompleteness.

2.4 Colours

As already mentioned, the number of objects detected in U_{300} is a relatively small fraction of the total number of galaxies in the catalog. This obviously prevents a detailed analysis of the full $U_{300} - V_{606}$ distribution at faint V_{606} magnitudes, where for most of the objects only an upper limit to the ultraviolet flux is available.

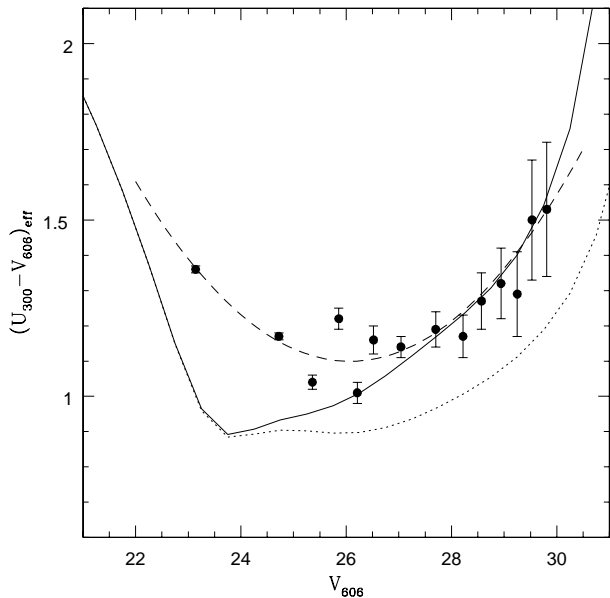


Figure 6. Colour-magnitude diagram, $(U-V)_{eff}$ vs. V_{606} (filled circles). The six brighter bins contain 80 galaxies each, while the fainter bins contains 240 objects. The dashed curve represents a quadratic fit to the data to $V_{606} < 29$. *Solid line*: prediction from a PLE model including the attenuation by the IGM. *Dotted line*: unattenuated PLE model.

It is possible, however, to use the measured fluxes after background subtraction for all the galaxies to get a statistical estimate on the average properties of the $U_{300} - V_{606}$ vs. V_{606} relation at much fainter V_{606} magnitudes than allowed by the U_{300} detections. We have therefore computed in each bin of V_{606} magnitude the total F300W and F606W fluxes as the sum of all the counts measured in individual galaxies, and have derived an “effective” colour for the entire population, $(U_{300} - V_{606})_{eff}$. This is not equal to the mean value, $\langle U_{300} - V_{606} \rangle$. For example, if the colour distribution were a gaussian with mean $\langle U_{300} - V_{606} \rangle$ and dispersion σ , it is easy to derive the relation $\langle U_{300} - V_{606} \rangle = (U_{300} - V_{606})_{eff} + 0.4605\sigma^2$.

Figure 6 shows the resulting colour-magnitude diagram. After an initial blueing trend, which is expected in PLE models (Pozzetti, Bruzual & Zamorani 1996), at fainter magnitudes galaxies become redder in $(U_{300} - V_{606})_{eff}$. This may be due to an increase in the fraction of high redshift galaxies or to a change in the colour properties of low redshift objects. As a test for distinguishing between these two alternative possibilities we have estimated the expected ultraviolet counts from the observed optical counts and the derived $(U_{300} - V_{606})_{eff}$ colours. The following input ingredients have been used:

- i) the observed $\log N(m) - V_{606}$ relation, which we fitted as a double power-law with $\gamma_b = 0.32$, $\gamma_f = 0.17$, and $V_c = 25.5$;
- ii) an assumed gaussian distribution for $U_{300} - V_{606}$ with a mean such that the resulting $(U_{300} - V_{606})_{eff}$ is equal to the fitted value in each V_{606} bin;
- iii) two different assumptions for the fraction, $f(V_{606})$, of high redshift galaxies in 0.5 magnitude bins: $f_1(V_{606}) = 0$ and $f_2(V_{606}) = 0.097 \times (V_{606} - 22.68)$ for $23 \leq V_{606} \leq 27$, as obtained by the dropout technique (see § 2.2). At fainter flux

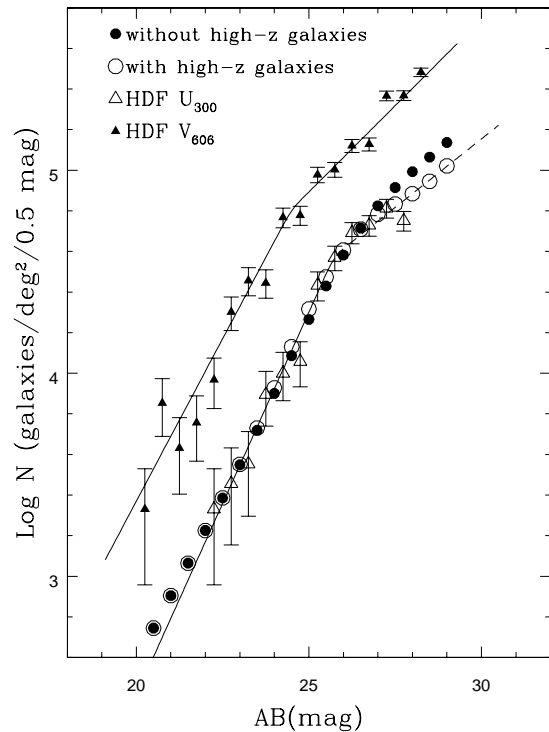


Figure 7. U_{300} (open triangles) and V_{606} (filled triangles) number-magnitude relation from the HDF data. Simulated ultraviolet counts are also plotted, with (open circles) and without (filled circles) the inclusion of high- z galaxies (see text). The solid lines depict the best-fits to the V_{606} data and the U_{300} $N(m)$ relation, with the former brightened by 1 magnitude for clarity.

levels, where the dropout analysis fails, we have assumed that $f_2(V_{606})$ remains constant.

Figure 7 shows the results for the two cases. In the very simple approach followed here we have assigned the same colour, $U_{300} - V_{606} = 4$ mag, to all high redshift objects, which therefore contribute only a negligible fraction of the total measured U_{300} flux in each V_{606} bin. The $(U_{300} - V_{606})_{eff}$ colour for the low redshift galaxies is then recomputed by scaling the total measured V_{606} flux in each bin by $1 - f_2(V_{606})$. In the same figure we show the data points with error bars, the fit to the bright counts, and the fit at fainter magnitudes derived from the fluctuation analysis. The predicted ultraviolet $N(m)$ is significantly higher than what is allowed by the fluctuation analysis for $f = f_1$, while it is in excellent agreement with the fluctuation analysis for $f = f_2(V_{606})$.

We conclude that the results of our analyses, i.e. the fluctuation analysis on the U_{300} data, the colour selection of Lyman-break galaxies, the derivation of the $U_{300} - V_{606}$ effective colour as a function of V_{606} magnitude (and its application to the V_{606} counts to predict the expected ultraviolet counts), are all consistent with each other and with the idea that, at faint UV flux limits, there is a significant absorption-induced loss of sources in the HDF.

3 EXTRAGALACTIC BACKGROUND LIGHT

The extragalactic background light (EBL) is an indicator of the total optical luminosity of the universe. It can provide unique information on the origin of structures at early

Table 2. Integrated Galaxy Light

| λ (Å) | $AB(\text{range})$ | I_ν^a | σ^+ | σ^- |
|---------------|--------------------|-----------|------------|------------|
| 3600 | 18.0–28.0 | 0.35 | 0.07 | 0.05 |
| 4500 | 15.0–29.0 | 0.56 | 0.11 | 0.07 |
| 6700 | 15.0–29.5 | 1.49 | 0.27 | 0.20 |
| 8100 | 15.0–29.0 | 2.10 | 0.44 | 0.25 |
| 22000 | 12.0–25.5 | 5.81 | 1.50 | 0.89 |

a in units of 10^{-20} erg cm $^{-2}$ s $^{-1}$ Hz $^{-1}$ sr $^{-1}$.

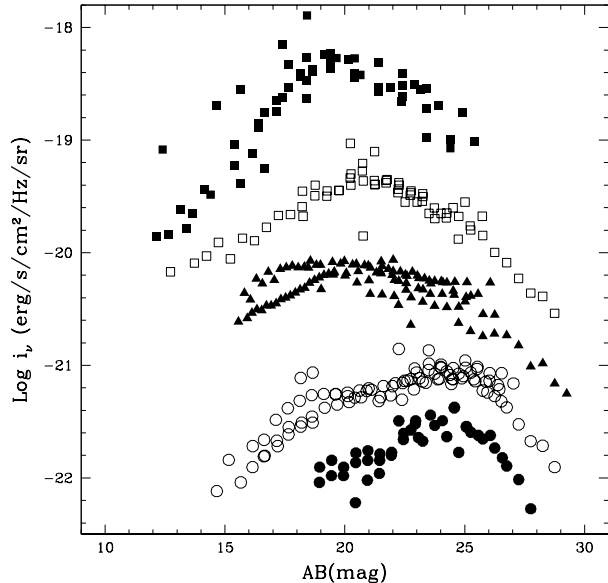


Figure 8. Extragalactic background light per magnitude bin as a function of U (filled circles), B (open circles), V (filled triangles), I (open squares) and K (filled squares) magnitudes. For clarity, the B , V , I and K values have been multiplied by a factor of 2, 8, 30, and 100, respectively.

epochs, as the cumulative emission from pregalactic, protogalactic, and evolving galactic systems is expected to be recorded in this background (Tyson 1995). The contribution to the EBL from discrete objects can be calculated directly by integrating the flux times the differential number counts down to the detection threshold. We have used the compilation of ground-based and HDF data shown in Figure 2, and the compilation of K -band data shown in Figure 3 of Pozzetti et al. (1996), to compute the EBL at $3500 \lesssim \lambda \lesssim 22000 \text{ \AA}$. The results are listed in Table 2, along with the magnitude range of integration and the estimated 1σ error bars, which arise mostly from field-to-field variations in the numbers of relatively bright galaxies.

Because of the flattening at faint magnitudes of the $N(m)$ differential counts, most of the contribution to the EBL comes from relatively bright galaxies. This is clearly seen in Figure 8, where the function $i_\nu = 10^{-0.4(m+48.6)} \times N(m)$ is plotted against apparent magnitude in all bands. While the differential contribution to the EBL increases at bright fluxes, where the slope of the ground-based counts is relatively steep, it appears that the HDF survey, reaching the limits beyond which the counts flatten below 0.40, has achieved the sensitivity to capture the bulk of the extragalactic light from discrete sources. An extrapolation of the

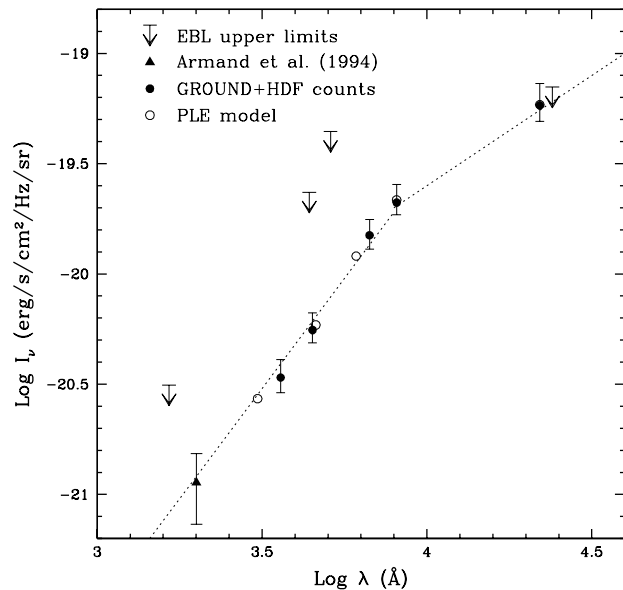


Figure 9. Spectrum of the extragalactic background light as derived from a compilation of ground-based and space-based galaxy counts. Also plotted are the 90% all-sky-photometry upper limits from Bowyer (1991), Toller (1983), Dube et al. (1977, 1979), and Boughn et al. (1986). For clarity, the upper limit at $\lambda = 2.2 \mu\text{m}$ has been plotted at $2.4 \mu\text{m}$. Dotted line: broken power-law fit to the EBL spectrum.

observed $N(m)$ to brighter and/or fainter magnitudes would typically increase the integrated light by less than 20%. The spectrum of the EBL (including a UV point at 2000 \AA from Armand, Milliard, & Deharveng 1994) is shown in Figure 9, and can be well described by a broken power-law: $I_\nu = 1.9 \times 10^{-20} (\lambda/8000 \text{ \AA})^2$ erg cm $^{-2}$ s $^{-1}$ Hz $^{-1}$ sr $^{-1}$ from 2000 to 8000 \AA , and $I_\nu = 1.9 \times 10^{-20} (\lambda/8000 \text{ \AA})$ erg cm $^{-2}$ s $^{-1}$ Hz $^{-1}$ sr $^{-1}$ from 8000 to 22000 \AA . Several diffuse EBL upper limits – set by all-sky photometry – are also plotted. While in the optical/UV these are from 3 to 5 times higher than the contribution from known galaxies, the upper limit to the total diffuse K -band EBL lies only slightly above the summed flux from discrete objects.

4 COMPARISON BETWEEN THE DATA AND A STANDARD PLE MODEL

Qualitatively, the effects of the inclusion of intergalactic attenuation in any galaxy evolution model are easily described. By severely obscuring sources above $z \approx 2$ in the ultraviolet band, and above $z \approx 4$ in the blue, the ubiquitous presence of H I along the line of sight to distant sources gives effectively origin to galaxy samples that are volume-limited in these bands. This truncates the galaxy redshift distribution and causes a flattening, more pronounced in the bluest filters, of the slope of the number-magnitude relation. The differential effect in the various bandpasses could then, at least in principle, allow us to discriminate between different models. Indeed, a more pronounced flattening of the ultraviolet $N(m)$ relative to the counts at longer wavelengths is likely to flag the presence of a significant population of faint high- z objects. Moreover, objects close to the redshift limit set by the opacity of the intergalactic medium should appear

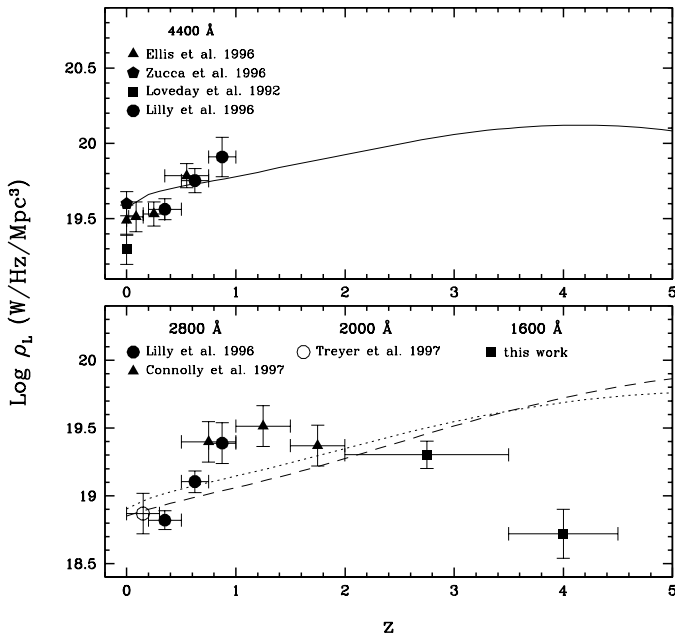


Figure 10. Integrated luminosity per unit comoving volume as a function of redshift ($H_0 = 50 \text{ km s}^{-1} \text{ Mpc}^{-1}$, $q_0 = 0.05$). The sources of the data points are indicated in each panel. The curves show the luminosity density predicted by a PLE model at 4400 Å (solid line), 2800 Å (dotted line), and 1600 Å (dashed line).

quite redder.

In the following, we shall briefly examine the predictions of a standard pure-luminosity-evolution model, modified by the inclusion of the effects of intergalactic attenuation, and compare them with the results obtained from the HDF data. Such a model, which assumes a single redshift of formation (z_f) for all galaxies and a open universe, was shown by Pozzetti et al. (1996) to be able to reproduce, with different degrees of accuracy, most of the properties of faint field galaxies as derived from ground-based surveys. The differential galaxy counts as a functions of AB magnitude, as expected within a PLE model with $z_f = 6.3$, are shown in Figure 2. Intervening absorption begins to affect the ultraviolet counts at $U_{300} \gtrsim 25$ mag, where the predicted slope flattens to $\gamma \lesssim 0.3$. By $U_{300} \sim 29$, the PLE model including intergalactic attenuation has $\gamma \sim 0$ and predicts about 2 times less galaxies than expected in a transparent universe. The median redshift for the global galaxy distribution is $z_{med} \simeq 2$ at $(U_{300}, B_{450}, V_{606}, I_{814}) \simeq (29, 28, 27, 26)$. At intermediate magnitudes ($20 \lesssim AB \lesssim 25$), luminosity evolution causes a blueing trend in the mean colours (Pozzetti et al. 1996). Only at fainter flux levels ($\gtrsim 25$ mag) the effect of the IGM becomes significant, producing a clear trend towards redder ultraviolet-optical colours with increasing magnitude (Figure 6).

Overall, the adopted PLE model appears to provide a rather acceptable fit to both the ground-based and HDF galaxy counts (Figure 2), as well as to the EBL spectrum (Figure 9). It produces, in good agreement with the observations, a flattening at faint magnitudes which is more significant at shorter wavelengths. The predicted turn-over in the U_{300} bandpass is, however, sharper than allowed by

the fluctuation analysis, due to the presence of too many high- z galaxies in the model relative to data. While, as shown in Figure 6, the inferred reddening in $(U_{300} - V_{606})_{eff}$ at magnitudes fainter than $V_{606} = 26$ is consistent with what expected in a PLE model (note how the same model without attenuation predicts bluer colours than observed in this magnitude range), at brighter flux levels ($23 < V_{606} < 26$) the synthetic colours appear to be too blue. The reason for this difference between model and data is not clear.

In Figure 4, the predicted fractions of colour-selected U_{300} and B_{450} dropouts versus V_{606} magnitude are compared with the HDF observations. While the relative numbers of ultraviolet dropouts are consistent with the PLE prediction, there is a clear deficit of observed B_{450} dropouts relative to the model. As already pointed out by Ferguson & Babul (1997), it appears that a major problem of a PLE scenario is the large number of predicted galaxies at high redshifts.

This is confirmed by Figure 10, which shows a comparison between the observed luminosity densities as a function of redshift at different wavelengths and the predictions of the PLE model. At 4400 Å the model generates a luminosity density which increases only slightly with redshift for $z < 1$. The local comoving emissivities derived from the data by different authors show a large spread, of order a factor two, although the most recent observations (Ellis et al. 1996; Zucca et al. 1997) suggest a higher normalization than that obtained by Loveday et al. (1992). If this is correct, the data are consistent with no or weak evolution up to $z \sim 0.3$. A rapid evolution, not reproduced by the model, is instead required by the data in the range $0.3 < z < 1.0$, both in the blue and at ultraviolet wavelengths. At higher redshifts, the model is in good agreement with the luminosity density we have derived at 1600 Å in the range $2.0 < z < 3.5$, while it is higher than the observations by a factor ~ 10 in the interval $3.5 < z < 4.5$.

5 CONCLUSIONS

By applying a simple fluctuation analysis to the U_{300} data, we have obtained an estimate of the slope of the ultraviolet counts, down to more than a magnitude fainter than the last data point published by Williams et al. (1996). The derived UV number-magnitude relation agrees with what has been obtained by convolving the observed V_{606} counts with the derived $(U_{300} - V_{606})_{eff}$ vs. V_{606} relation, and assuming a fraction of high- z galaxies consistent with the results of the dropout colour technique. All these results convincingly show that the effects of an IGM absorption-induced loss of sources are significant at faint ultraviolet magnitudes ($AB > 27$). At flux levels of $AB \approx 27$ mag, about 7% of the sources in U_{300} , 30% in B_{450} , and 35% in V_{606} are Lyman-break “dropouts”, i.e., candidate star-forming galaxies at $z > 2$.

The rest-frame UV luminosity densities we derive at high redshifts using a maximum likelihood reconstruction of the true colour distribution are in good agreement with previous estimates (Madau et al. 1996; Madau 1997). We note that the existing data do not necessarily require a sharp peak of the ultraviolet luminosity density at $z \sim 1.5$, but may also be consistent with an approximately constant value over a redshift range as large as $0.8 \lesssim z \lesssim 3.0$.

From our dropout sample we have also derived the M_{1600} luminosity functions in the redshift intervals $2.0 < z < 3.5$ and $3.5 < z < 4.5$. The LF is reasonably well defined in the lower redshift interval, and can be described by a Schechter function with parameters $\alpha = -1.3$, $M_{1600}^* = -21.7$ and $\Phi^* = 0.8 \times 10^{-3} \text{ Mpc}^{-3}$. The same α and M_{1600}^* values, but with a normalization four times lower, provide a good fit to the blue dropouts at higher redshifts. Both functions extend to brighter magnitudes than the local 2000 Å LF recently derived by Treyer et al. (1997).

A detailed comparison between a simple PLE galaxy evolution model and the available ground-based and HDF data shows that the model fails to reproduce all the observed properties of faint field galaxies. While able to fit reasonably well the observed number counts, colours, and the fraction of ultraviolet dropouts at $\langle z \rangle \sim 2.75$, this PLE model overpredicts by about one order of magnitude the number of blue dropouts at $z > 3.5$ and the corresponding rest-frame UV luminosity density. Moreover, it fails to account for the steep observed trend of the galaxy emissivity observed in the redshift range $0.3 < z < 1$ at all wavelengths. The modeling of the emission history of the galaxy population at late epochs is outside the scope of this paper; we note here that Madau, Pozzetti & Dickinson (1997) have recently shown that the rapid variation of the luminosity density at small redshifts can be well fit by a simple stellar evolution model, defined by time-dependent star formation rate per unit comoving volume and a universal initial mass function. At high redshifts, since in our PLE model a significant fraction of the emitted light is due to elliptical galaxies just after their first massive starburst phase, a possible solution to the observed discrepancy could be obtained by assuming that a significant amount of dust obscures the early evolution of these massive systems. A similar conclusion has been reached by Franceschini et al (1997) in their analysis of a K-band selected sample of early-type galaxies in the HDF. Approximate consistency with the $\langle z \rangle \sim 4$ observations would require a dust extinction of $E(B-V) \sim 0.2 \div 0.23$ for SMC-type dust and the empirical extinction-law of Calzetti, Kinney & Storchi-Bergman (1994), respectively, corresponding to an ultraviolet extinction of about a factor of 10. The current estimates of the ultraviolet extinction for the star-forming galaxies at $z \sim 3$ are still very uncertain and range from about 2 (Pettini et al. 1997) to more than 10 (Meurer et al. 1997). If such a large amount of dust, consistent with the observations of local starburst galaxies (Calzetti 1997), was present in star-forming objects at high- z , it would absorb a large fraction of the optical-UV light and re-emit it in the far infrared band (see, for example, the models described in detail in Mazzei, De Zotti & Xu 1994). In this case, the amount of star formation derived from our and similar dropout analyses should only be considered as a lower limit. Preliminary observations of the HDF with ISO (Rowan-Robinson et al. 1997) have revealed about a dozen far-IR (6.7 and $15 \mu\text{m}$) sources, identified with optical galaxies. By fitting the spectra of these galaxies from the ultraviolet to the far-IR, Rowan-Robinson et al. (1997) have derived star formation rates significantly higher than those derived from the UV fluxes detected with HST. On the other hand, Madau et al. (1997) show that a model with a large amount of hidden star formation at early epochs will overproduce the cosmic metallicity at high- z as sampled by

the damped Lyman- α systems (Pettini et al. 1997). The results discussed above demonstrate the great potential of IR observations for complementing the information provided by the rest-frame ultraviolet and for helping our understanding of the nature of high- z galaxies.

ACKNOWLEDGMENTS

We have benefited from discussions with M. Dickinson, A. Fruchter, and M. Romaniello. Support for this work was provided by NASA through grant AR-06337.10-94A from the Space Telescope Science Institute, which is operated by the Association of Universities for Research in Astronomy, Inc., under NASA contract NAS5-26555, and by ASI through contracts 95-RS-152 and ARS-96-70.

REFERENCES

- Armand C., Milliard B., Deharveng J.M., 1994, *A&A*, 284,12
 Avni Y., Soltan A., Tananbaum H., Zamorani G., 1980, *ApJ*, 238, 800
 Avni Y., Tananbaum H. 1986, *ApJ*, 305, 83
 Bruzual G.A., Charlot S., 1993, *ApJ*, 405, 538
 Boughn S.P., Saulson P.R., Uson J.M., 1986, *ApJ*, 301, 17
 Bowyer S., 1991, *ARA&A*, 29, 59
 Calzetti D., Kinney A.L., Storchi-Bergmann T., 1994, *ApJ*, 429, 582
 Calzetti D., 1997, in W.H. Waller, ed, *The Ultraviolet Universe at Low and High redshift*. AIP Press (in press)
 Cohen J.G., Cowie L. L., Hogg D. W., Songaila A., Blandford R. D., Hu E. M., Snopbell P., 1996, *ApJ*, 471, L5
 Connolly A.J., Szalay A.S., Dickinson M., SubbaRao M.U., Brunner R.J., 1997, *ApJ Letters* (in press)
 Cowie L.L., Songaila A., Hu E.M., Cohen J.G., 1996, *AJ*, 112, 839
 Crampton D., Le Fèvre O., Lilly S.J., Hammer F., 1995, *ApJ*, 455, 96
 Dube R.R., Wickes W.W., Wilkinson D.T., 1977, *ApJ*, 215, L51
 Dube R.R., Wickes W.W., Wilkinson D.T., 1979, *ApJ*, 232, 333
 Ellis R.S., Colless M., Broadhurst T., Heyl J., Glazebrook K., 1996, *MNRAS*, 280, 235
 Feigelson E.D., 1992, in Feigelson E.D. Babu J.G., eds, *Statistical Challenges in Modern Astronomy*, Springer Verlag, New York, p.221
 Feigelson E.D., Nelson P.I., 1985, *ApJ*, 293, 192
 Ferguson H., Babul A., 1997, *MNRAS* (in press)
 Franceschini A., Silva L., Granato G.L., Bressan A., Danese L., 1997, *ApJ* (submitted) (astro-ph/9707064)
 Gardner J.P., Sharples R.M., Carrasco B.E., Frenk C.S., 1996, *MNRAS*, 282, L1
 Glazebrook K., Peacock J.A., L. Miller, Collins C.A., 1995, *MNRAS*, 275, 169
 Guhathakurta P., Tyson J.A., Majewski S. R., 1990, *ApJ*, 357, L9
 Hall P., Mackay C.B., 1984, *MNRAS*, 210, 979
 Heyl J., Colless M., Ellis R.S., Broadhurst T., 1996, astro-ph/9610036
 Jones L.R., Fong R., Shanks T., Ellis R.S., Peterson B.A., 1991, *MNRAS*, 249, 481
 Koo D.C., 1986, *ApJ*, 311, 651
 Koo D., Gronwall C., Bruzual G.A., 1993, *ApJ*, 415, L21
 La Valley M., Isobe T., Feigelson E.D., 1992, *BAAS*, 24, 839
 Lilly S.J., Cowie L.L., Gardner J.P., 1991, *ApJ*, 369, 79
 Lilly S.J., Hammer F., Le Fèvre O., Crampton D., 1995a, *ApJ*, 455, 75

- Lilly S.J., Le Fevre O., Hammer F., Crampton D., 1996, ApJ, 460, L1
- Loveday J., Peterson B.A., Efstathiou G., Maddox S.J., 1992, ApJ, 390, 338
- Lowenthal, J. D., et al. 1997, ApJ, 481, 673
- Madau P., 1995, ApJ, 441,18
- Madau P., 1997, in S.S. Holt, G.L. Mundy, eds, Star Formation Near and Far. AIP: New York, p.481
- Madau P., Ferguson H. C., Dickinson M. E., Giavalisco M., Steidel C. C., Fruchter A. 1996, MNRAS, 283, 1388
- Madau P., Pozzetti L., Dickinson, M. E., 1997, ApJ (in press) (astro-ph/9708220)
- Maddox S.J., Sutherland W.J., Efstathiou G., Loveday J., Peterson B.A., 1990, MNRAS, 247, Short Comm., 1p
- Magri C., Haynes M., Forman W., Jones C., Giovannelli R. 1988, ApJ, 333, 136
- Majewski S.R., 1989, in Frenk C.S. et al., eds, The Epoch of Galaxy Formation. Kluwer, Dordrecht, p. 85
- Mazzei P., De Zotti G., Xu C., 1994, Ap.J., 422, 81
- Metcalfe N., Shanks T., Fong R., Jones L.R., 1991, MNRAS, 249, 498
- Metcalfe N., Shanks T., Fong R., Roche N., 1995, MNRAS, 273, 257
- Metcalfe N., Shanks T., Campos A., Fong R., Gardner J.P. 1996, Nature, 383, 236
- Meurer G.R., Heckman, T.M., Lehnert, M.D., Leitherer, C., Lowenthal, J., 1997, AJ, 114, 54
- Oke J.B., 1974, ApJS, 27, 21
- Pettini M., Smith L., King D.L., Hunstead R.W., 1997, ApJ (in press)
- Pettini M., Steidel C.C., Dickinson M., Kellogg M., Giavalisco M., Adelberger K.L., 1997, in W. Waller, ed, The Ultraviolet Universe at Low and High Redshift, AIP (in press) (astro-ph/9707200)
- Picard A., 1991, AJ, 102, 445
- Pozzetti L., Bruzual G.A., Zamorani G. 1996, MNRAS, 281, 953
- Rowan-Robinson M. et al. 1997, MNRAS (in press)
- Schmitt J.H.M.M. 1985, ApJ, 293, 178
- Smail I., Hogg D.W., Yan L., Cohen J.G., 1995 ApJ, 449, L105
- Steidel C.C., Hamilton D., 1992, AJ, 104, 941
- Steidel C.C., Hamilton D., 1993, AJ, 105, 2017
- Steidel C.C., Pettini M., Hamilton D. 1995, AJ, 110, 2519
- Steidel C.C., Giavalisco M., Pettini M., Dickinson M., Adelberger K. 1996a, ApJ, 462, L17
- Steidel C.C., Giavalisco M., Dickinson M., Adelberger K. 1996b, AJ, 112, 352
- Stevenson P.R.F., Shanks T., Fong R., 1986, in Chiosi C., Renzini A., eds, Spectral Evolution of Galaxies. Reidel, Dordrecht, p. 439
- Toller G.N., 1983, ApJ, 266, L79
- Tyson J.A., 1988, AJ, 96, 1
- Tyson J.A., 1995, in Calzetti D., Livio M., Madau P., eds, Extragalactic Background radiation, Cambridge University Press, p.103
- Treyer M.A., Ellis R.S., Milliard B., Donas J., 1997, in W.H. Waller, ed, The Ultraviolet Universe at Low and High redshift. AIP Press (in press)
- Yee H.K.C., Green R.F., 1987, ApJ, 319, 28
- Weir N., 1994, Ph.D. thesis, California Institute of Technology
- Williams et al. , 1996, AJ, 112, 1335
- Yoshii Y., Peterson B.A., 1994, ApJ, 436, 551